RS2016 Symposium

7th International Symposium on In-Situ Rock Stress

May 10-12, 2016
Tampere, Finland

Suomen Kalliomekaniikkatoimikunta
Finnish National Group of ISRM

Proceedings

ISRM Specialized Conference 2016

7th International Symposium on In-Situ Rock Stress

May 10-12, 2016, Tampere, Finland

Symposium proceedings

Editors

Erik Johansson

Ville Raasakka

Organizers

The Finnish National Group of ISRM

Finnish Association of Civil Engineers RIL

Organizing committee

Erik Johansson, Chair
Juha Antikainen
Matti Hakala
Harri Kuula
Risto Niinimäki
Jukka Pöllä
Ville Raasakka
Mikael Rinne
Topias Siren
Antti Sorsa
Pekka Särkkä
Kirsti Tikkanen
Lauri Uotinen
Teemu Vehmaskoski

International Advisory Committee

Daniel Ask, Sweden
Francois Cornet, France
Rolf Christiansson, Sweden
Phil Dight, Australia
Xian-Ting Feng, China
John Hudson, UK
Takatoshi Ito, Japan
Kimmo Kemppainen, Finland
Errol De Kock, South-Africa
Luis Lamas, Portugal
Charlie Li, Norway
Derek Martin, Canada
Ki-Bok Min, South Korea
Jonny Sjöberg, Sweden
Ove Stephansson, Germany
Resat Ulusay, Turkey
Ernesto Villaescusa, Australia
Koji Yamamoto, Japan
Arno Zang, Germany

ISBN 978-951-758-606-1

ISSN 0356-9403

PREFACE

The 7th In-Situ Rock Stress Symposium (RS2016) is a natural continuation of the in-situ rock stress topic, which is of great importance to most rock engineering projects. In spite of the numerous research and development projects that have been undertaken in the subject of rock stresses, a great deal remains to be achieved in order to confidently establish the stress field and its variation at a particular site, plus the alteration to the stress field as construction proceeds. We have much improved stress measurement methods and associated 3-D computer programs—and the development is moving fast. Hence, we are delighted to see so many rock stress practitioners, modellers, designers and contractors at this RS2016 Symposium. We are sure that the 7th Symposium will contain much new material and is an excellent forum for presenting your work, keeping up to date with developments, and networking.

The RS2016 Symposium is organized by the Finnish National Group of ISRM and the Finnish Association of Civil Engineers RIL. There have been six previous International Symposia on the rock stress topic, starting in 1976 in Sydney, Australia, and with the most recent one being held in Sendai, Japan, in 2013. The Rock Stress Symposia are currently arranged approximately every third year and belong to series of the ISRM Specialized Conferences.

The RS2016 is arranged in the beautiful city of Tampere, Finland, which is the third largest city in Finland and currently very active in the field of underground projects. Why we are now in Finland is because of the large amount of rock engineering construction and the fact that rock stresses play an important role in the design of Finnish rock engineering projects—even in the shallow underground facilities. Although the high horizontal stresses can be utilized in stabilizing rock caverns, such high stresses can also cause rock damage around the rock facilities, so understanding the stress field and designing accordingly is one of the keys to success.

The 7th In-Situ Rock Stress Symposium consists of five keynote presentations, 59 technical papers from 13 countries, two technical excursions and a Post-symposium excursion to Olkiluoto nuclear waste repository site. Technical papers which are orally presented are allocated to eight symposium themes: 1) Rock stress measurements with different methods, 2) Interpretation and analysis of results; 3) Case studies (nuclear waste disposal, mining, civil engineering); 4) Regional stress fields; 5) Seismicity and rock stress; 6) New, innovated stress measurement methods; 7) Rock structures and rock stress; and 8) Stress modeling. On the behalf of the Organizing Committee I wish to thank all the authors for their papers and making this high quality symposium possible. Also, I want to thank all the participants and the sponsor companies for their support. Looking forward to interesting discussions!

Erik Johansson

Chair of the Organizing Committee

RS2016

NUMERICAL MODELLING OF EARTHQUAKES AND INDUCED SEISMICITY UNDER VARIOUS IN SITU STRESS CONDITIONS AT FORSMARK, SWEDEN, THE SITE FOR A FINAL REPOSITORY OF SPENT NUCLEAR FUEL

Jeoung Seok Yoon (jsyoon@gfz-potsdam.de)
Ove Stephansson and Arno Zang
Helmholtz Centre Potsdam GFZ German Research Centre for Geosciences
Germany

Ki-Bok Min
Seoul National University
South Korea

Flavio Lanaro
SSM Swedish Radiation Safety Authority
Sweden

ABSTRACT

This study concerns dynamic simulations of earthquakes and the seismicity associated with induced slip of pre-existing fractures in the rock mass for a repository for spent nuclear fuel planned to be constructed at Forsmark, Sweden. We use Particle Flow Code 2D (PFC^{2D}) to model the repository volume that contains the faults and the pre-existing fracture system. The heterogeneous structure of the faults and the pre-existing fracture system are explicitly modelled in PFC^{2D} using the smooth joint model. Earthquake at a fault is simulated by instantaneous release of the strain energy stored along the fault after build-up of the rock stresses. The release produces earthquakes and the seismic waves propagate and attenuate through the model. The earthquakes are simulated under different present day in situ stress conditions and under estimated future glacial cycles of Weichselian type. In particular, the time of ice cover and related forebulge, maximum thickness of the ice cover, and the retreat of the ice cover are considered. Modelling results demonstrate that the magnitudes and the stress drops of the induced seismic events associated with fracture slip tend to be the largest under stress condition of high anisotropy, in other words, where the ratio of the maximum and the minimum horizontal stresses is large. Among the seven tested in situ stress conditions, the occurrence of an earthquake under the stress condition at the time of forebulge in front of the ice cover is found to produce the largest induced moment magnitude (M ~3).

KEYWORDS

Nuclear waste repository, Forsmark, Earthquake, In situ stress, Glacial cycle, Fracture slip, Induced seismicity, Stress drop, Spent Fuel

INTRODUCTION

To be able to assess the long term safety of a repository for radioactive waste or spent nuclear fuel against earthquakes that can possibly occur at a nearby fault, reliable estimates of the seismic magnitudes and of the response of the pre-existing fracture system in the repository rock mass are essential. The safety assessment of as such a complex geological system can only be done by numerical modelling. The knowledge of the in situ stress conditions at the site and at the depth of the repository is essential because stresses constitute the boundary conditions to the model and accumulate energy in the geological structures. Moreover, as the nuclear waste can have a radioactive half-life of several thousand years, the stress conditions to be considered for the long term safety assessment of the repository should include conditions, not only for the present day, but also for possible future glacial periods. This study dynamically simulates an earthquake on selected faults and investigates the induced seismicity associated with slip induced by the earthquake of the natural pre-existing

fractures. The rock mass for a repository for spent nuclear fuel planned by the Swedish Nuclear Fuel and Waste Management Company (SKB) to be constructed at Forsmark, Sweden, and presently under regulatory review for obtaining a construction license, is chosen for such analyses. Dynamic modelling of an earthquake is done by using Particle Flow Code 2D (PFC^{2D}) (Itasca, 2009). We look into the response of the natural pre-existing fracture system in terms of magnitudes and stress drops associated with target fracture slip induced by the earthquake seismic loading. We simulate an earthquake at one specific fault near the repository under various stress conditions and estimate for which stress condition the earthquake magnitude as well as the response of the fracture system are the largest.

THE FORSMARK REPOSITORY MODEL

The Forsmark repository model is generated based on the integrated geological model provided by Stephens et al. (2015) shown in Figure 1a. The geological model contains mostly two sets of deformation zones: zones with trace length at the ground surface greater than 3 km (in red) and zones with length smaller than 3 km (in blue). The geometry of the mapped deformation zones on the horizontal section at the depth of the repository is converted into a format readable by PFC^{2D}. The zones are replaced by a set of PFC's *smooth joints* (Mas Ivars et al., 2008 and 2011). The traces of the discrete fracture network (DFN), also called *target fractures*, are stochastically generated in 3D in a form of disks and cut at repository depth (Yoon et al., 2014b; shown in red in Figure 1b). The deformation zones in the model are steeply dipping and are explicitly modelled with their full trace length. When modelled with the smooth joint model, a deformation zone is not represented as a continuous plane, but as a collection shorter smooth joints as shown in Figure 1c. It is considered reasonable to represent a heterogeneous object such as faults, deformation zones or fractures in this way since they are not planar but rather undulated or stepped at large scale.

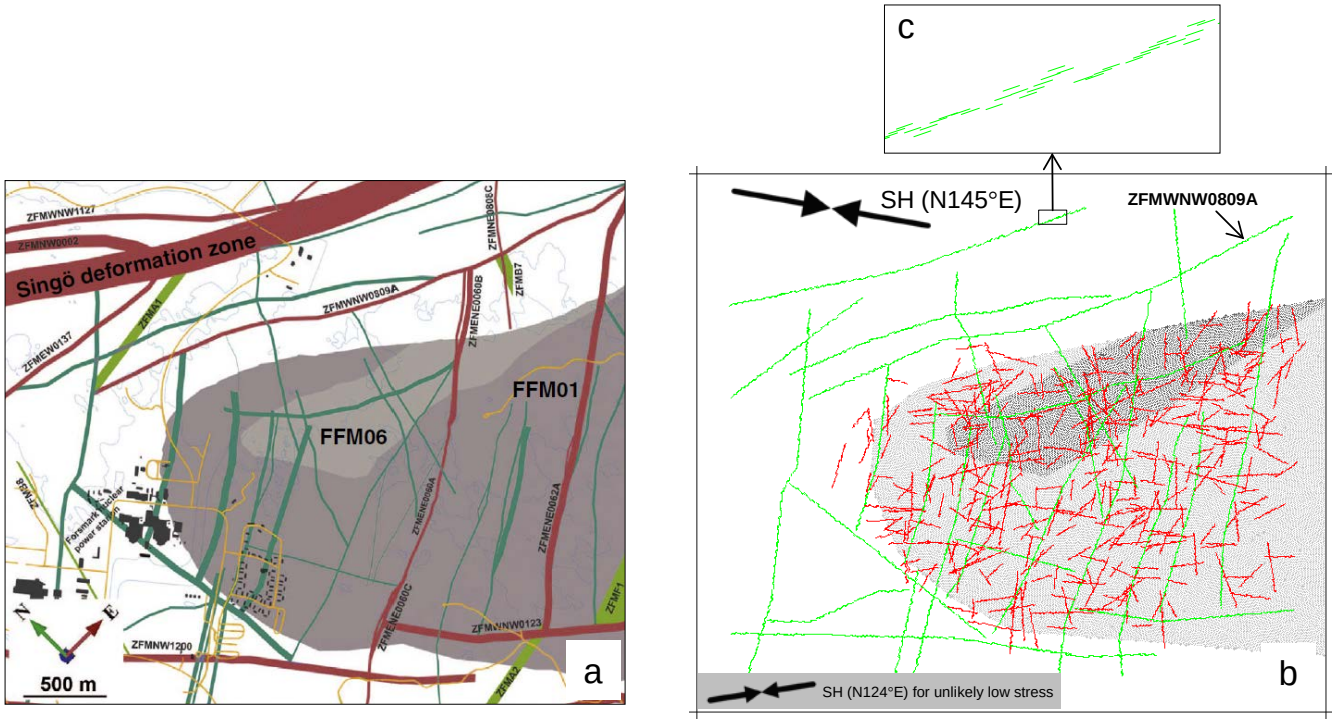

Figure 1. (a) Integrated geological model of the Forsmark site at the depth of the repository (Stephens et al. 2015); (b) the Forsmark repository model generated with PFC^{2D} containing the deformation zones (green) and the target fractures (red). The arrows indicate the orientation of the maximum horizontal stress of the most likely stress condition. For the *unlikely low* stress condition the direction of the maximum horizontal stress is N124°E. In the box, a partial trace of a deformation zone is enlarged in (c).

IN SITU AND FUTURE STRESS CONDITIONS

Seven different stress conditions are considered in the simulations. The first three boundary stresses in the modelling are estimated for the present day and include the following: *most likely* (Martin, 2007), *unlikely high* (SKB, 2009), and *unlikely low* determined by the hydraulic method (Ask et al., 2007). The second four boundary stresses are estimations for the future glacial period assuming a Weichselian glacial cycle (Lund et al., 2009), which includes a *first maximum ice cover*, *forebulge*, *second maximum ice cover* and *ice cover retreat*. Figure 2 shows the glacially induced stress increments of the maximum (σ_H, red curve) and the minimum (σ_h, green curve) horizontal stresses due to the evolution of ice cover thickness (black curve). The stress increments at the four selected times are added to the stress components under the most likely stress condition assumed in the repository model. Table 1 lists the two horizontal stress components for the seven different stress fields with orientation of the maximum horizontal stress and ratio of maximum and minimum horizontal stresses. As the numerical model represents the horizontal section at the repository depth, vertical stresses in the out-of-plane dimension are not considered. Moreover the pore fluid pressure at the repository depth of about 4.6 MPa is not taken into account. Therefore, the stresses presented in Table 1 are total stress. Stresses are applied to the repository model (Figure 1b) by controlling the velocity of the layers of particles at the outer boundaries of the model until the stress components monitored at several locations in the model match in magnitude and orientation with the assumed set of stresses (i.e. the black arrow in Figure 1b). The orientation of the maximum horizontal stress for the present day *unlikely low* stress condition is N124°E (Figure 1b).

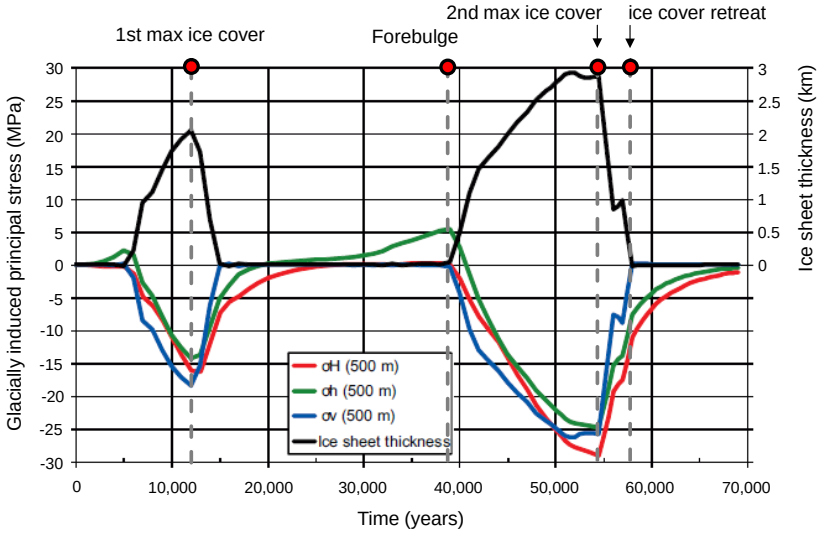

Figure 2. Glacially induced increments of the rock stresses at the repository depth during a Weichselian glacial cycle (modified from Figure 4-12 in Hökmark et al., 2010).

Table 1. Horizontal rock stresses for different stress models at the repository depth, orientation of the maximum horizontal stress, deviatoric stress and stress ratio at Forsmark.

Stress models	σ_H (MPa)	σ_h (MPa)	σ_H orientation	σ_H-σ_h (MPa)	σ_H/σ_h	References
Present most likely	40	22	N145°E	18	1.82	Martin (2007)
Present unlikely high	55	35	N145°E	20	1.57	SKB (2009)
Present unlikely low	20	10	N124°E	10	2.00	Ask et al. (2007)
Glacial 1st max ice cover	56	36	N145°E	20	1.56	Hökmark et al. (2010)
Glacial forebulge	40	17	N145°E	23	2.35	Hökmark et al. (2010)
Glacial 2nd max ice cover	69	47	N145°E	22	1.47	Hökmark et al. (2010)
Glacial ice cover retreat	53	31	N145°E	22	1.71	Hökmark et al. (2010)

MODELLING OF EARTHQUAKES

An earthquake is simulated by releasing the strain energy that is accumulated along the trace of the fault or deformation zone during the application of rock stresses. In order to accumulate strain energy in the smooth joints along the deformation zone that will host an earthquake, the bond strength of the smooth joints is multiplied by a factor of 1000. Thereafter the model is compressed until the stresses σ_H and σ_h in the model and the orientation of σ_H match the target stresses listed in Table 1. Deformation zone ZFMWNW0809A east of the repository area is selected for the earthquake modelling (see Figure 1). The release of the strain energy is simulated by lowering the tensile and cohesive bond strength of the smooth joints of the zone and this leads to slip along the deformation zone (Yoon et al., 2014b). The friction and dilation angles of the smooth joint are lowered to 10% of their original values, i.e. from 35° to 3.5°. This mimics a fault rupturing process where the fault surface asperities that contribute to friction and dilation are lost during the dynamic slip. Upon releasing the strain energy, the seismic moment and the moment magnitude of the seismic events are computed using the moment tensor method by Hazzard and Young (2002; 2004), which was extended by Yoon et al. (2014a) to be able to handle the smooth joint failure. Seismic wave are generated from the activated deformation zone and propagate, reflect, refract due to the other deformation zones and attenuates by damping inside the model.

SEISMICITY ASSOCIATED WITH FRACTURE SLIP

The seismic wave generated by an earthquake at the deformation zone travels through the repository volume and induces slip on other deformation zones and the target fractures. The seismic moment, M_0, associated with slip, d, of a target fracture with length, L, is computed using equation (1) by Aki (1966) and the moment magnitude M_w using equation (2) by Hanks and Kanamori (1979):

$$M_0 = GAd \quad (1)$$

$$M_w = 2/3\log(M_0)-6 \quad (2)$$

where, G is the shear modulus (in this study 30 GPa), A is the surface area of the fracture (πr^2), r is the radius of the fracture assumed to be half the length L.

The radiated seismic energy (E_{sr}) of an induced seismic event is calculated using equation (3) by Gutenberg and Richter (1956) as a function of the moment magnitude M_w:

$$\log(E_{sr}) = 4.8+1.5M_w \quad (3)$$

The stress drop $\Delta\sigma$ is computed assuming that the seismicity of a circular source and using equation (4) by Keilis-Borok (1959):

$$\Delta\sigma = (7\pi/16)G(d/r) \quad (4)$$

RESULTS AND DISCUSSION

The spatial distribution of the stress drops associated with fracture slip induced by an earthquake at deformation zone ZFMWNW0809A under (a) the present day most likely stress condition and (b) the glacially induced stress condition at the time of ice forebulge are shown in Figure 3. Locations of the earthquake hypocentres are indicated by the star and the zone ZFMWNW0809A is indicated red. It is assumed that the largest slip occurs at the fracture centre and therefore the symbols of the stress drops are shown at that position and coloured according to their 10 based logarithm. This means that a symbol coloured with red has a stress drop between 3.2 MPa to 10 MPa. For clarity, the circles showing the stress drops are also scaled according to the stress drop values. The largest symbol shown in Figure 3b corresponds to approximately 8.7 MPa stress drop.

The results demonstrate that the stress drops are in general large near the earthquake hypocenter (Figure 3). It also shows that the larger the distance from the hypocentre the smaller the stress drops. However, there are seismic events at the opposite end of the repository with respect to the earthquake hypocentre where the stress drops are higher than expected, see Figure 3a. This trend is more distinct in Figure 3b for the glacially induced stress condition at the time of ice cover forebulge. Although the magnitudes of the simulated earthquakes are almost the same, the stress drops are in general larger for the time of at the time of forebulge than those for the present day most likely stress condition.

The distribution of larger stress drops for the glacial forebulge stress condition can be explained by the larger stress anisotropy induced by the reduction of the minimum horizontal stress (σ_h) (Figure 2), which consequently leads to higher ratio σ_H/σ_h and differential stress $\sigma_H-\sigma_h$ (see Table 1).

Clustering of the induced seismicity with large stress drops at the opposite side of the repository with respect to the triggering earthquake hypocentre indicates that the location is under state of higher local shear stress. However, as this study concerns response of only one realization of DFN induced by an earthquake simulated at one specific deformation zone (ZFMWNW0809A), it is necessary to run some more simulations with different realizations of DFN to study the spatial variation in the location of the seismicity clusters with large shear drops. Such information may be used for the design of a repository layout in such way that those areas can be avoided for construction of deposition tunnels.

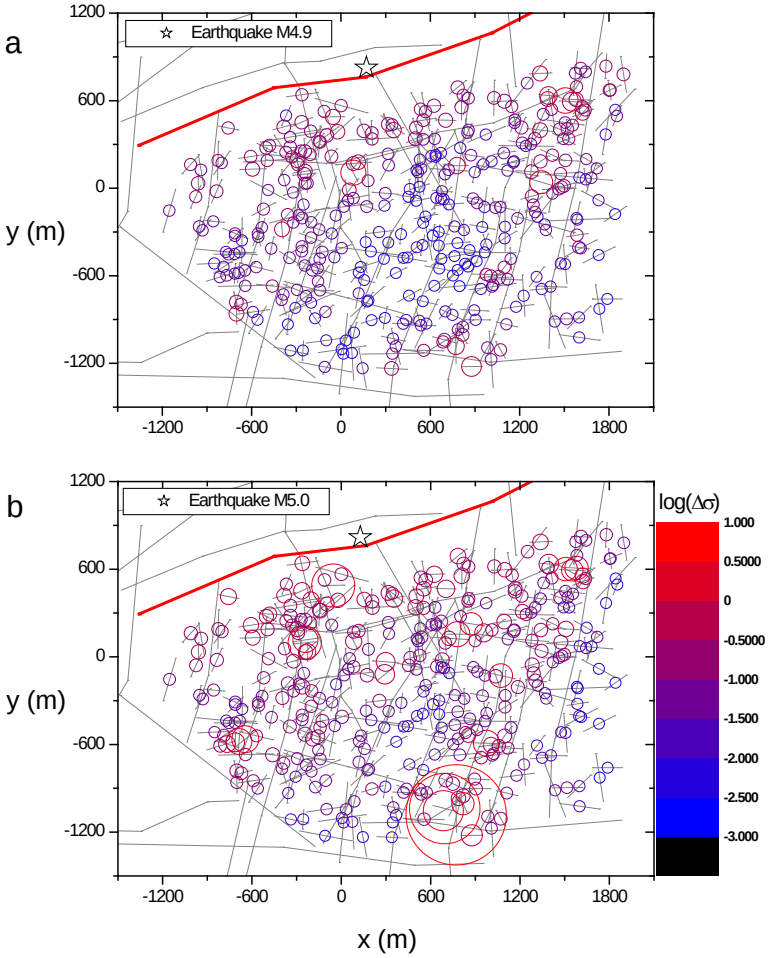

Figure 3. Distribution of the stress drops associated with target fracture slip induced by an earthquake at deformation zone ZFMWNW0809A in red under: (a) the present day most likely stress condition and (b) the glacially induced stress condition at the time of ice forebulge. Stress drop symbols are coloured according their values on the $\log_{10}$-scale on the right hand side. The stars show the hypocenter of the simulated earthquake.

Table 2 lists other modelling results which include: earthquake activation magnitude (M_{EQ}), the largest magnitude of the induced seismicity associated with fracture slip (M_{max}), the largest stress drop ($\Delta\sigma_{max}$) and the average stress drop ($\Delta\sigma_{avg}$) associated with the fracture slip, the b values of the magnitude-frequency distribution of the induced seismicity according to Gutenberg-Richter scaling relation, and the ratio of the seismic radiated energy from the induced seismicity associated with the fracture slip (E_{sr}) and the seismic energy provided by an earthquake (E_{EQ}) equivalent to the earthquake seismic moment.

The earthquake activation magnitudes tend to be proportional to the magnitudes of the initial stresses. This can be seen from the activation magnitude of an earthquake under the unlikely low stress condition (M_{EQ}=4.4) where σ_H=20 MPa and σ_h=10 MPa. The largest magnitude of the induced seismicity M_{max}=3.0 under the stress condition of glacial forebulge and the second largest magnitude M_{max}=2.6 under the present unlikely minimum stress condition. The largest stress drops are dependent on the applied stress ratio.

The induced seismicity magnitudes and their cumulative frequency relations are investigated to calculate the Gutenberg-Richter b values using the Maximum Likelihood Method in equation (5) (Aki, 1965, Bender, 1983):

$$b = 0.434/(M_{avg}-M_c) \quad (5)$$

where M_{avg} is the average magnitude and M_c is the magnitude completeness assumed to be 1.0.

As listed in Table 2, except the glacial forebulge stress condition, the calculated b values are larger than 1. The seismicity induced by an earthquake under glacial forebulge condition shows relatively low b (0.91). More anisotropic state of stress made by the effect of the glacial forebulge leads to increase of shear stress on most of the fractures. The results are consistent with Urbancic et al. (1992) and Wyss (1973) that an increase of the applied shear stress or effective stress results in a decrease of b-value. Compared to the typical b-values of induced seismic events in worldwide Enhanced Geothermal System (b~2; Grünthal, 2014), the b-value of the simulated seismic events induced by the tectonic earthquakes shows a similar range, except for the glacial forebulge stress condition.

Table 2. Modelling results: Earthquake activation magnitudes at the host deformation zone (M_{EQ}), maximum moment magnitude of the induced seismicity at target fractures (M_{max}), maximum stress drop ($\Delta\sigma_{max}$) and average stress drop ($\Delta\sigma_{avg}$) of the induced seismicity, the Gutenberg-Richter b value and the ratio between the cumulative radiated seismic energy (E_{sr}) of the induced seismicity and the earthquake energy (E_{EQ}).

Stress models	**M_{EQ}**	**M_{max}**	**$\Delta\sigma_{max}$**	**$\Delta\sigma_{avg}$**	**b-value**	**E_{sr}/E_{EQ} (%)**
Present most likely (Fig.3a)	4.9	2.3	1.4	0.1	1.74	$2.0*10^{-5}$
Present unlikely high	4.8	2.3	1.1	0.1	1.71	$2.3*10^{-5}$
Present unlikely low	4.4	2.6	5.8	0.1	2.50	$1.0*10^{-4}$
Glacial 1st max ice cover	4.8	2.2	1.2	0.1	1.71	$2.1*10^{-5}$
Glacial forebulge (Fig.3b)	5.0	3.0	8.7	0.3	0.91	$2.9*10^{-5}$
Glacial 2nd max ice cover	4.8	2.4	1.4	0.1	2.23	$2.4*10^{-5}$
Glacial ice retreat	4.9	2.4	2.1	0.1	1.71	$2.2*10^{-5}$

Figure 4 shows the relation between the seismic energy of the simulated earthquakes and the sum of the radiated seismic energy of the induced seismicity associated to them. The dashed lines represent the ratios of the radiated seismic energy (E_{sr}) and the earthquake energy E_{EQ} (same as the seismic moment M_0). The energy ratios simulated in this study are between $2.0\cdot10^{-5}$% and $1.0\cdot10^{-4}$%. For reference, we provide the data from world-wide Enhanced Geothermal Systems, waste water disposal in USA and Canadian shale gas fracturing (modified from Zang et al., 2013). The hydraulic energy inputs are in general smaller than the earthquake energy simulated in this study. However, in terms of the ratio between the radiated seismic energy and the input seismic energy, the radiated energy of the earthquake induced seismic events are maximum 5 orders less than those seismic events induced in the Enhanced Geothermal Systems. It should be noted that the data plotted in Figure 4 are field observations, whereas the red dots data are from the earthquake simulation in this study. Also, it should be noted that the radiated seismicity energy in the numerical models is limited to 346 fractures that are

stochastically generated from the given length range (125 m to 600 m). In reality, the number of pre-existing fractures that would respond to the earthquake should be far greater than 346, and the ratio could increase. However, it is not likely that the radiated seismic energy will reach 10^{13} Joule as the case of Denver earthquake (Data pt.16) where massive waste water injection in Colorado USA resulted in activation of nearby fault (Healy et al., 1970, Hsieh and Bredehoeft, 1981, Nicholson and Wesson, 1992).

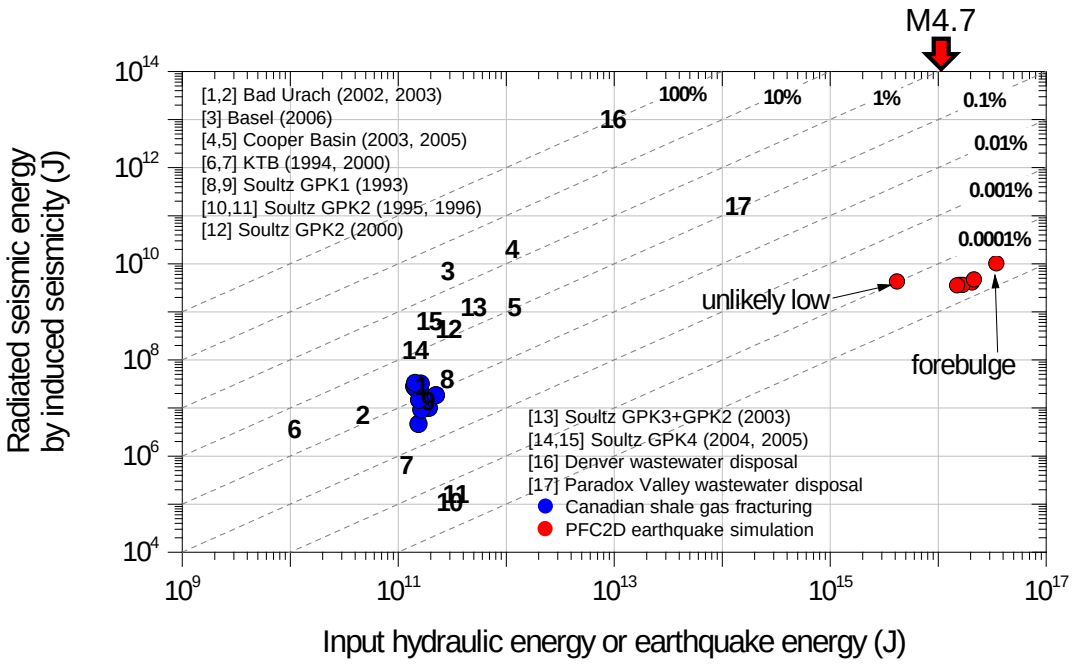

Figure 4. Relation between the hydraulic energy or earthquake energy of the simulated earthquakes and the radiated seismic energy of the induced seismicity (red dots). For reference, data from Enhanced Geothermal Systems, waste water disposal in US and Canadian shale gas fracturing (blue dots) and the radiated seismic energy of the induced seismicity are provided for reference (modified from Zang et al., 2013).

SUMMARY AND CONCLUSIONS

This study presents numerical modelling of earthquake at Forsmark, Sweden, at the site for the planned final repository for spent nuclear fuel and radioactive waste. Earthquakes at one of the nearby deformation zones, specifically ZFMWNW0809A, are simulated under assumptions of various stress conditions at the depth of the repository. Three stress conditions for the present day (most likely, unlikely high, unlikely low stress) and four stress conditions that can evolve during the future glacial period (first maximum ice cover, forebulge, second maximum ice cover and the ice retreat) simulating a Weichselian type of glaciation are taken into account. Particle Flow Code 2D is used where the earthquake is simulated by releasing the strain energy stored along the trace of the earthquake fault. Slip of the fractures due to the earthquake seismic loading is analyzed and the seismicity magnitudes and stress drops associated with the fracture slip are calculated.

Irrespective of the stress conditions in the present day or during a Weichselian type of glacial period, the magnitude of the simulated earthquake at ZFMWNW0809A is M5 or below. Stress drops associated with the seismic slip of the target fractures are in average 0.1 MPa. The Gutenberg-Richter b values computed on the magnitude-frequency distributions of the induced seismicity are larger than 1 and some cases are even large than 2. The seismicity associated with the fracture slip induced by the earthquake tends to be larger in terms of stress drop and magnitude under higher anisotropic stress state which is likely to be the case at the time of glacial forebulge. Among the seven tested stress conditions, the slip potential of the fractures and the seismicity

associated with slip tends to be the largest during the time of glacial forebulge where the state of in situ stress condition becomes more anisotropic. To be conclusive on the integrity of the repository against an earthquake loading, we suggest that more simulation runs are necessary, especially for the glacial forebulge stress condition using different realizations of DFN and earthquake at different deformation zones.

ACKNOWLEDGEMENTS

The results are presented by courtesy of the Swedish Radiation Safety Authority (SSM) and have been produced in the context of a geomechanical study by GFZ German Research Centre for Geosciences (SSM2014-3668) in collaboration with Seoul National University, South Korea (SSM2013-3839).

REFERENCES

Aki, K. (1965). *Maximum likelihood estimate of b in the formula logN=a-bM and its confidence limits*. Bulletin of the Earthquake Research Institute 43, 237-239.

Aki, K. (1966). *Generation and propagation of G-waves from the Niigata earthquake of June 16, 1964. Part 2: Estimation of earthquake moment, released energy, and stress-strain drop from the G-wave spectrum*. Bulletin of the Earthquake Reseach Institute 44, 73-88.

Ask, D., Cornet, F., Brunet, C., Fontbonne, F. (2007). *Forsmark site investigation – Stress measurements with hydraulic methods in boreholes KFM07A, KFM07C, KFM08A, KFM09A and KFM09B*. SKB P-07-206, Swedish Nuclear Fuel and Waste Management Co.

Bender, B. (1983). *Maximum likelihood estimation of b values for magnitude grouped data*. Bulletin of the Seismological Society of America 73, 831-851.

Boroumand, N., Eaton D.W. (2012). *Comparing energy calculations: Hydraulic fracturing and microseismic monitoring*. GeoConventions 2012: Vision.

Grünthal, G. (2014). Induced seismicity related to geothermal projects versus natural tectonic earthquakes and other types of induced seismic events in Central Europe. Geothermics 52, 22-35.

Gutenberg, B., Richter, C.F. (1956). *Earthquake magnitude, intensity, energy and acceleration (second paper)*. Bulletin of the Seismological Society of America 46, 105-145.

Hanks, T.C., Kanamori, H. (1979). *A moment magnitude scale*. J Geophys Res 84(B5), 2348-2350.

Hazzard, J:F., Young, R.P. (2002). *Moment tensors and micromechanical models*. Tectonophysics 356, 181-197.

Hazzard, J.F., Young, R.P. (2004). *Dynamic modelling of induced seismicity*. International Journal of Rock Mechanics & Mining Sciences 41, 1365-1376.

Healy, J.H., Hamilton, R.M., Raleigh, C.B. (1970). *Earthquakes induced by fluid injection and explosion*. Tectonophysics 9, 205-214.

Hökmark, H., Lönnqvist, M., Fälth, B. (2010). *THM-issues in repository rock – Thermal, mechanica, thermo-mechanical and hydro-mechanical evolution of the rock at the Forsmark and Laxemar sites*. SKB TR-10-23, Swedish Nuclear Fuel and Waste Management Co.

Hsieh, P.A., Bredehoeft, J.D. (1981). *A reservoir analysis of the Denver earthquakes: A case of induced seismicity*. Journal of Geophysical Research 86, 903-920.

Keilis-Borok, V.I. (1959). *On estimation of the displacement in an earthquake source and of source dimensions*. Annali de Geofisica 12, 205-214.

Lund, B., Schmidt, P., Hieronymus, C. (2009). *Stress evolution and fault stability during the Weichselian glacial cycle*. SKB TR-09-15, Swedish Nuclear Fuel and Waste Management Co.

Martin, C.D. (2007). *Quantifying in situ stress magnitude and orientatios for Forsmark. Forsmark Stage 2.2*. SKB R-07-26, Swedish Nuclear Fuel and Waste Management Co.

Mas Ivars, D., Potyondy, D.O., Pierce, M., Cundall, P.A. (2008). *The smooth-joint contact model*. 8th World Congress on Computational Mechanics (WCCM8) & 5th European Congress on Computational Methods in Applied Sciences and Engineering (ECCOMAS 2008), June 30 – July 5, 2008, Venice, Italy.

Mas Ivars, D., Pierce, M.E., Darcel, C., Reyes-Montes, J., Potyondy, D.O., Young, R.P., Cundall, P.A. (2011). *The synthetic rock mass approach for jointed rock mass modelling*. International Journal of Rock Mechanics & Minining Sciences 48, 219-244.

Mukuhira, Y., Asanuma, H., Miitsuma, H., Häring, M.O. (2013). *Characteristics of large-magnitude microseismic events recorded during and after stimulation of a geothermal reservoir at Basel, Switzerland*. Gothermics 45, 1-17.

Nicholson, C., Wesson, R.L. (1992). *Trigered Earthquakes and Deep Well Activities*. Pure and Applied Geophysics 139, 72-86.

SKB. (2009). *Site engineering report Forsmark. Guidelines for underground design Step D2*. SKB R-08-83, Swedish Nuclear Fuel and Waste management Co.

Stephens, M.B., Follin, S., Petersson, J., Isaksson, H., Juhlin, C., Simeonov, A. (2015). *Review of the deterministic modelling of deformation zones and fracture domains at the site proposed for a spent nuclear fuel repository, Sweden, and consequeces of structural anisotropy*. Tectonophysics 653, 68-94.

Urbancic, T.I., Trifu, C.-I., Long, J.M., Young, R.P. (1992). *Space-time Correlations of b Values with Stress Release*. Pure and Applied Geophysics 139, 449-462.

Wyss, M. (1973). *Towards a Physical Understaning of the Earthquake Frequency Distribution*. Geophysical Jorunal of the Royal Astronomical Society 31, 341-359.

Yoon, J.S., Zang, A., Stephansson, O. (2014a). *Numerical investigateion on optimized stimulation of intact and naturally fractured deep geothermal reservoirs using hydro-mechanical coupled discrete particles joints model*. Geothermics 52, 165-184.

Yoon, J.S., Stephansson, O., Min, K.-B. (2014b). *Relation between earthquake magnitude, fracture length and fracture shear displacemetn in the KBS-3 repository at Forsmark – Main Review Phase*. SSM Technical Note 2014:59, Swedish Radiation Safety Authority.

Zang, A., Yoon, J.S., Stephansson, O., Heidbach, O. (2013). *Fatigue hydraulic fracturing by cyclic reservoir treatment enhances permeability and reduces induced seismicity*. Geophysical Journal International 195, 1282-1287.